Autumn School on Modern Methods in High Frequency Spectroscopy, Reinhardsbrunn, East Germany, November 2-6, 1981

Conf-8111143--1

TIME-RESOLVED PULSED EPR: MICROWAVE AND OPTICAL DETECTION

A. D. Trifunac and J. P. Smith

Chemistry Division
Argonne National Laboratory
Argonne, Illinois 60439
USA

CONF-8111143--1

DE83 007853

ABSTRACT

Time-resolved pulsed EPR spectrometers are described. EPR spectra, kinetic profiles, and relaxation studies are used to illustrate some capabilities of the pulsed EPR experiment. Optical detection of time-resolved EPR spectra of radical ion pairs is used to study radical-ion recombination kinetics, recombination pathways and the structure of radical anions and cations.

INTRODUCTION

The study of many areas of chemistry involves investigation of short lived intermediates. In this last decade, we have witnessed an inexorable expansion of scientific tools which allow us to probe ever shorter time intervals in chemical reactions. A vast area of chemistry deals with the reactions of transient paramagnetic intermediates. It is to this area that we focus here. We will illustrate how we can develop ways to study short lived radicals in liquids by magnetic resonance methods.

Any study of transient paramagnetic species in solution is closely tied to the available methods of creating radicals and the time resolution of the method chosen for their detection. The intense pulsed lasers, e.g., nitrogen and more recently excimer lasers, can be used to create substantial concentrations (up to $\sim 10^{-4}$ M) of radicals in several nanoseconds. Pulse radiolysis utilizing short and intense electron beam pulses has been around longer and substantial radical concentrations ($\sim 10^{-3}$ M) are obtainable.

Why are we interested in the magnetic resonance tools, when neither sensitivity nor time resolution of EPR and NMR can equal the capabilities of optical detection methods? The limitations of magnetic resonance tools are offset by the ability of magnetic resonance to provide more definitive information on the identity and structure of the paramagnetic intermediates. As we will illustrate here, much can be done to make substantial improvements in both time resolution and the sensitivity of the time resolved magnetic resonance methods.

While we have developed several time resolved EPR and NMR experiments for the study of transient radicals in liquids, we focus here on the EPR developments.

DISCLAIMER

METHOD

At first continuous wave (CW) EPR was used to study transient radicals. High frequency field modulation and more recently no field modulation ("direct detection") EPR has been successfully used to study paramagnetic transients (1). While CW-direct detection EPR is still a very popular tool for the study of kinetics at a time scale ~1 μsec, if we wish to study radical dynamics at shorter times we often benefit by using pulsed microwaves. As we will illustrate, the use of pulsed microwaves, i.e., spin echo method, has many advantages of the CW-EPR approach. The absence of the microwave field (H_1) during observation in the spin echo method results in the major simplification of the kinetic analysis of transient magnetization (M_z) bypassing problems due to magnetic field inhomogeneity, and cavity disturbance at times close to the electron beam or laser pulse (2,3).

We will consider here several experiments where EPR spectra of transient radicals or radical ions, kinetics and relaxation are studied using one, two, or three microwave pulses. The optically detected EPR study of radical ions utilizes a single microwave pulse as we shall illustrate later.

The two pulse (spin echo) sequence (microwave detection) which is used to obtain either the EPR spectra or transient radical kinetics is illustrated in Figure 1.

The transient magnetization created by either electron beam or laser pulse is sampled by the 90-τ-180-τ-echo sequence. When this two-microwave pulse sequence is started at time t after the electron beam pulse and when the magnetic field is swept, one obtains EPR spectra of the transient (and stable) radicals present at that time (Figure 2). When the magnetic field is held at some fixed value corresponding to a particular

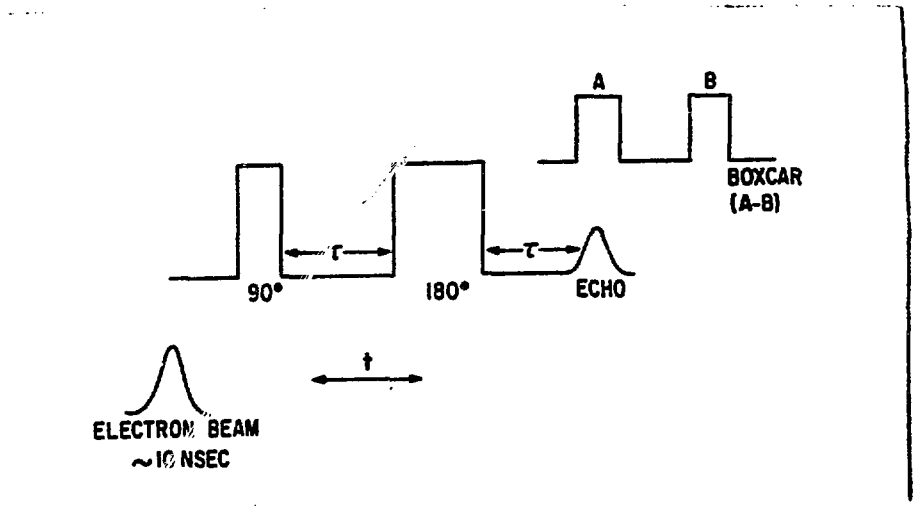

Figure 1. Timing between the electron beam (or laser) pulse, microwave pulses, and the observation (boxcar) gates.

Figure 2. Field swept EPR spectrum of $\cdot CH_2CO_2^-$ radical (pulse radiolysis) at 1 μsec after the electron beam pulse (B) central quartz signal reduced by beam-no beam subtraction.

EPR peak in EPR spectra in Figure 2, and the time between the creating pulse and the microwave pulse sequence is swept (t), the formation-decay of M_z is obtained (Figure 3).

The problem in the pulsed EPR-spin echo approach is that when obtaining spectra, all magnetization present (at the time when the 90° pulse is applied) is observed. In order to separate transient from steady state EPR species, special pulse sequences can be used which utilize phase shifting (Figure 4).

Spectra obtained with phase shifted pulse sequences are illustrated in Figures 5 and 6. For the study of kinetics, this is not necessary. The phase alterations of the second 180° pulse and "field spoiling" reduced FID interference which can be a problem when radicals with narrow lines are studied, i.e., when there is no substantial inhomogeneous broadening.

INSTRUMENTATION

The present state of microwave technology allows a straightforward design of the pulsed EPR spectrometer. Figure 7 illustrates the major components. The Gunn diode is a source of microwaves which are then switched as appropriate by the microwave switch #1 to produce desired pulses, amplified by the Traveling Wave Tube amplifier (TWT), routed to the cavity and then observed by the balanced mixer after amplification by a low noise GaAs FET amplifier or low noise TWT. Microwave

Figure 3. Kinetic traces (intensity arbitrary units) of the high field (HF) and low field (LF) $\cdot CH_2CO_2$ lines. Data (crosses) and least squares fitting (solid line). Dots indicate the calculated line through data points that were not used in the least squares fitting. Absolute normalized values of the intensities of the two lines are illustrated.

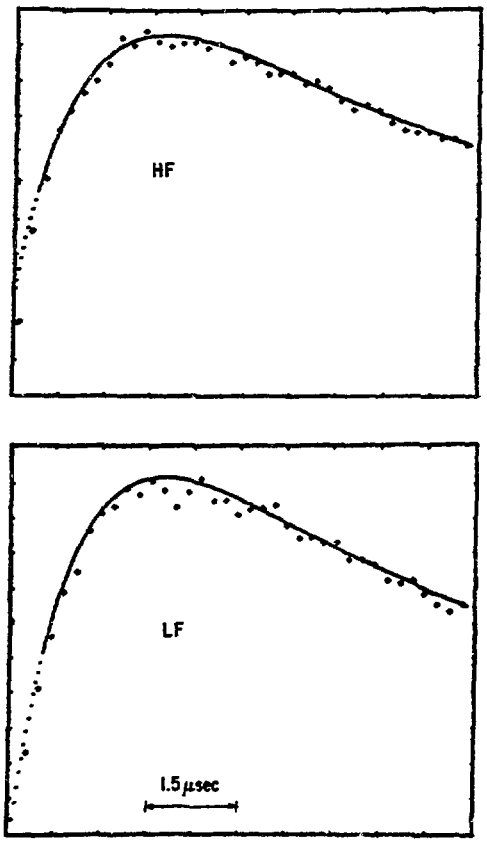

Figure 4. Schematic of phase shifted pulse sequences used to reduce FID interference from the second microwave pulse and accomplish beam-no beam subtraction.

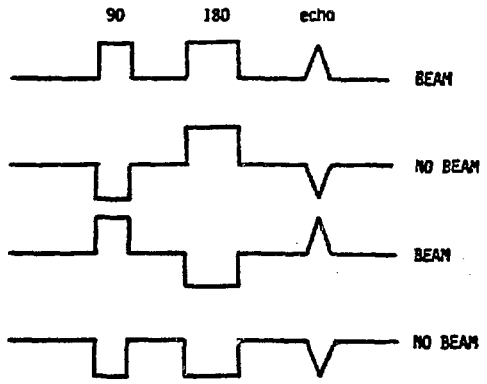

Figure 5. EPR spectra of $\cdot CH_2CO_2^-$ obtained without (top) and with (middle and bottom) phase shifted pulse sequences. Bottom spectrum represents a y-enlargement of the middle spectrum.

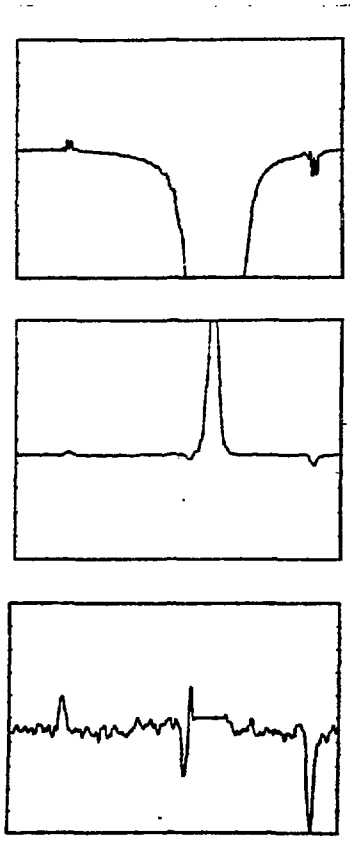

Figure 6. High field line of $\cdot CH_2CO_2^-$ radical (at 1 μsec). (A) No field spoil, no phase alteration; (B) phase alteration only; (C) field spoil and phase alteration; (D) field spoil only.

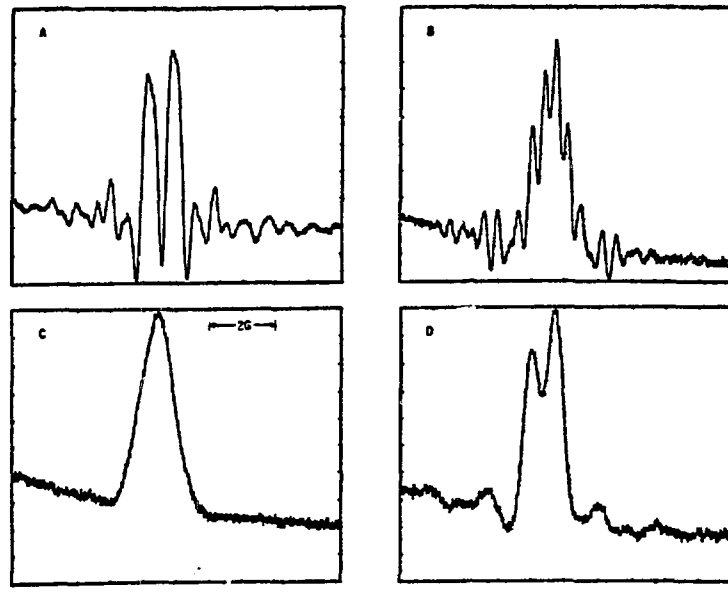

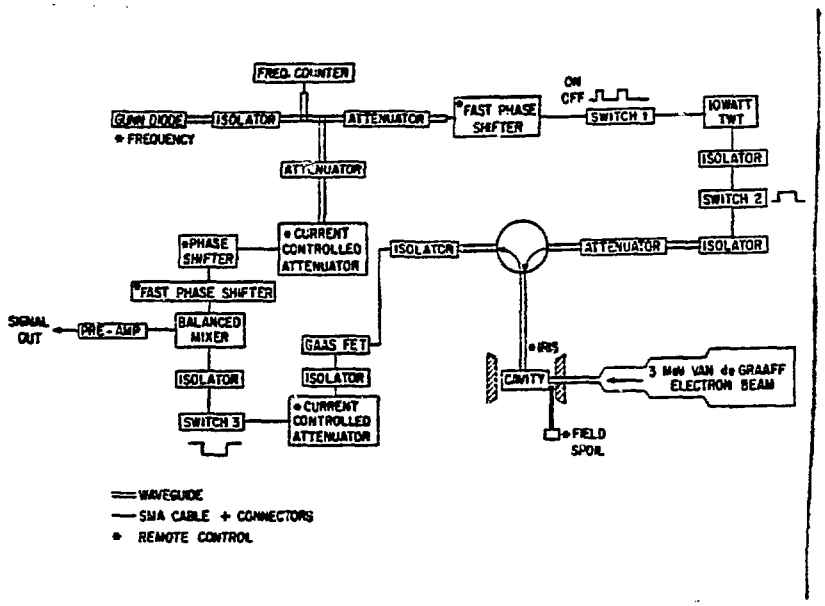

Figure 7. Schematic of the pulsed EPR experiment on the 3 MeV Van de Graff. The switching functions of the microwave switches are illustrated.

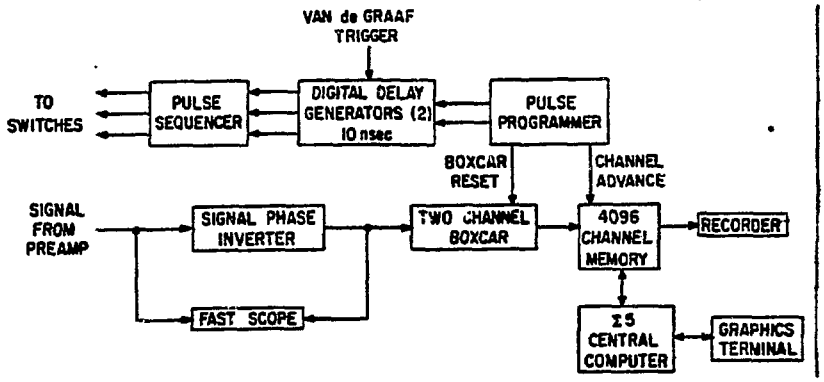

Figure 8. Timing, microwave switching and data acquisition schematic.

switches #2 and #3 serve to reduce the noise from the high power TWT from reaching the microwave detector.

The signal from the balanced mixer is amplified by a fast preamp and then sent to a boxcar averager and deposited in the memory of a time averaging computer. The layout of pulse control and signal handling is outlined in Figure 8.

Data Analysis: Acetate Radical CIDEP, Kinetics and Relaxation

The acetate radical is formed by OH· abstraction from acetate (2):

$$H_2O \xrightarrow{e^- \text{ beam}} \cdot OH \quad (1)$$

$$\cdot OH + CH_3CO_2^- \longrightarrow H_2O + \cdot CH_2CO_2^- \quad (2)$$

$$2 \cdot CH_2CO_2^- \longrightarrow (CH_2CO_2^-)_2 \quad (3)$$

and decays predominantly by the second order reaction (3). By observing the time dependence of the acetate radical signals, e.g., Figure 3, we obtain the time picture of $M_z(t)$. The analysis must include CIDEP, relaxation and chemical decay (3):

$$\dot{M}_z = -T_R(t)^{-1} M_z - T_1^{-1}(M_z - M_z^0) + \dot{E}(t) M_z^0 \quad (4)$$

The first term in Eq. 4 is the loss of magnetization by radical decay described by the lifetime $T_R(t)$ where:

$$T_R(t)^{-1} = -(\dot{R}/R) = -(d\ln R/dt) \quad (5)$$

The second term in Eq. 4 describes spin lattice relaxation towards its equilibrium value $M_z^0(t)$. The last term in Eq. 4 represents the pumping of the electron spin system by the chemical reaction. The data analysis is carried out by computer graphics utilizing an equation derived from Eq. 4. Typically one varies E (enhancement), T_1 (relaxation) time and T_c (second order half life) to obtain a reasonable fit. Curve fitting results are illustrated in Figures 3 and 9.

It should be noted that this curve fitting procedure involving up to three variables represents a considerable simplification over the curve fitting applied to CW-EPR data where additional parameters like H_1 are needed and where no reliable T_1 can be obtained.

The T_1 and T_2 can be independently obtained by utilizing three pulse sequences for T_1 (180-t-90-τ-180) or phase memory (90-τ-180) for T_2. In Figure 10 we illustrate the results of a study of T_1 dependence on radical concentration. There is a considerable reduction in T_1 (and T_2) at high radical concentrations. This observation can be explained by considering that there is an increasing number of nonreactive encounters at high radical concentrations leading to destruction of transient magnetization by Heisenberg spin exchange. These studies provide us with a way to measure the reactive/nonreactive radical encounter ratio by measuring radical kinetics and relaxation. This can provide a better picture of collisions between reactive radical pairs in solution.

Time Resolved Optically Detected EPR

The EPR spectra of radical ion pairs that recombine to produce an excited singlet state can be detected optically *via* observation of a resonant change in the intensity of fluorescence

Figure 9. High field line of $\cdot CH_2CO_2$ radical at three radical concentrations. Data (circles) and curve fit (solid line) are illustrated.

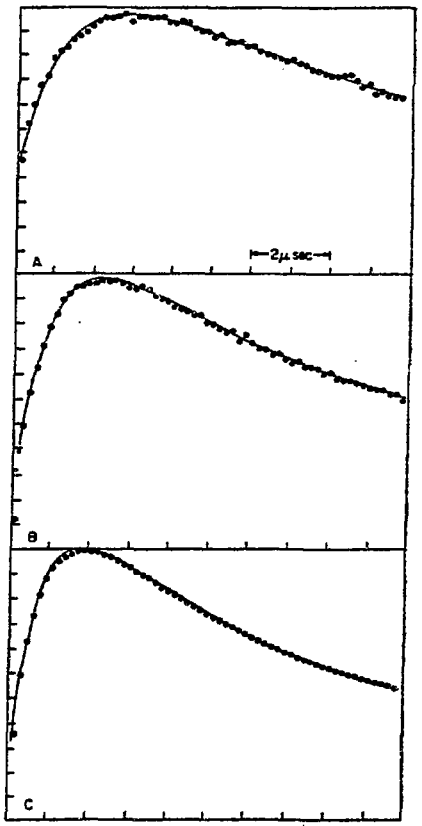

Figure 10. T_1 measurements at various $\cdot CH_2CO_2$ radical concentrations.
○ Asymptotic analysis.
△ Inversion recovery.
◇ Least squares computer fitting.

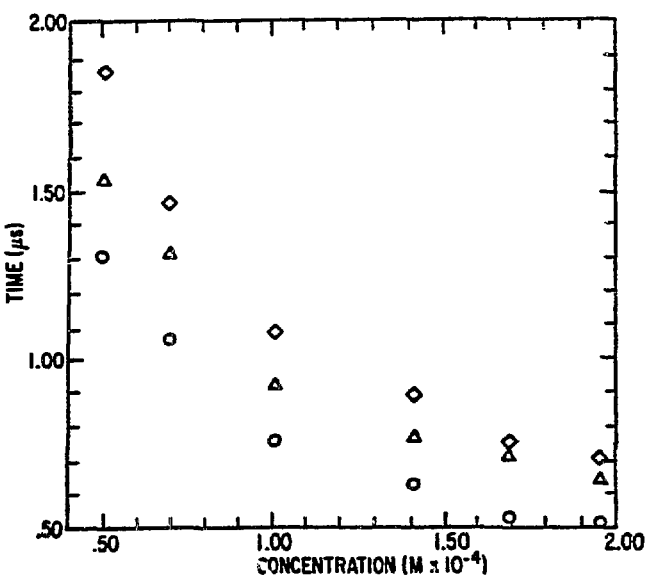

arising from ion recombination. This not only permits the application of magnetic resonance to some very interesting problems, but also results in a major improvement in the specificity and sensitivity of time resolved EPR (5,6).

One area of current research (7,8) is the radiation chemistry of hydrocarbon solutions of aromatic molecules. Radical ion recombination is a major source of the excited states produced by pulse radiolysis. The recombination pathways for excited state production are summarized in the following scheme where S and Ar represent the solvent and aromatic solute, respectively.

$$S \xrightarrow{e^- \text{ beam}} S^+ + e^- \quad (6)$$

$$S^+ + Ar \longrightarrow Ar^+ + S \quad (7)$$

$$e^- + Ar \longrightarrow Ar^- \quad (8)$$

$$Ar^+ + e^- \longrightarrow Ar^* \quad (9)$$

$$Ar^- + S^+ \longrightarrow Ar^* + S \quad (10)$$

$$Ar^- + Ar^+ \longrightarrow Ar^* + Ar \quad (11)$$

The primary products of ionization (6) are rapidly scavenged by solute molecules (7,8). Several ion recombination pathways (9-11) can then yield excited solute molecules. Experimentally, excited singlet state solutes are observed *via* fluorescence and excited triplet states are most conveniently observed by triplet-triplet absorption.

The EPR spectra of radical ion pairs can be detected by observation of a resonant decrease in fluorescence following the application of a single (30-100 ns) microwave pulse. Here we will discuss several features of the fluorescence detected magnetic resonance (FDMR) technique.

The experimental setup is illustrated in Figure 11. We use the same pulsed EPR spectrometer described in the previous section. The light from excited state emission escapes through a hole in the bottom of the cavity and is detected at a selected wavelength. At some time after irradiation, a single microwave pulse is applied and the fluorescence is sampled during a subsequent time window selected by a boxcar averager. An EPR spectrum corresponding to a superposition of the spectra of the isolated radical ions that recombined to produce the excited state is obtained by measuring the fluorescence intensity as a function of the applied magnetic field. For each spectrum, the positions of the microwave pulse and boxcar averager sampling window are fixed with respect to the time of irradiation. Typical FDMR spectra obtained for kinetic studies (Figure 12) consist of a single peak with no resolved hyperfine structure. In some cases, the hyperfine structure of the FDMR spectrum can be resolved through the use of long (250-500 ns), low power ($H_1 \leq$ 0.4 g) microwave pulses (Figure 13). Although the hyperfine

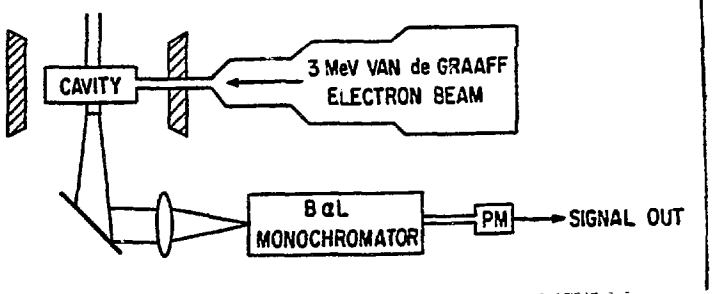

Figure 11. Experimental setup for optical detection of magnetic resonance showing the arrangement of the microwave cavity containing the sample cell; the electron beam and the light detection apparatus.

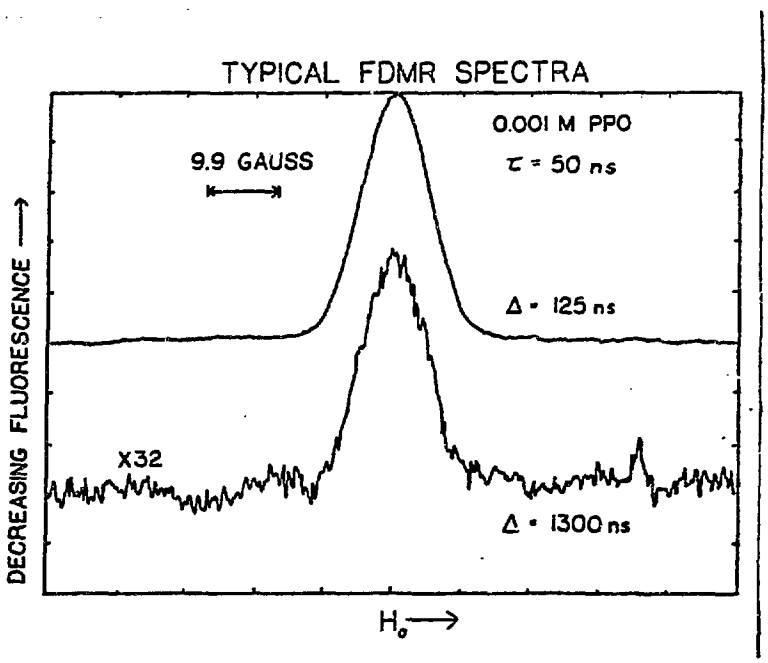

Figure 12. Typical FDMR spectra of 10^{-3} PPO (2,5 diphenyloxazole) in cyclohexane. The microwave pulse was applied from 0 to 100 ns after irradiation with a 5 ns electron beam pulse. The fluorescence was sampled from 75-175 ns (upper trace) or 1250-1350 ns (lower trace) after irradiation.

structure is resolved at the expense of some of the time resoluation and sensitivity of the FDMR method, the spectra obtained in this way can provide useful data on the identity and structure of the radical ion precursors of excited states in more complex chemical systems. A plot of integrated FDMR intensity vs. time, obtained from a series of spectra similar to those in Figure 12, provides information about radical ion pair spin

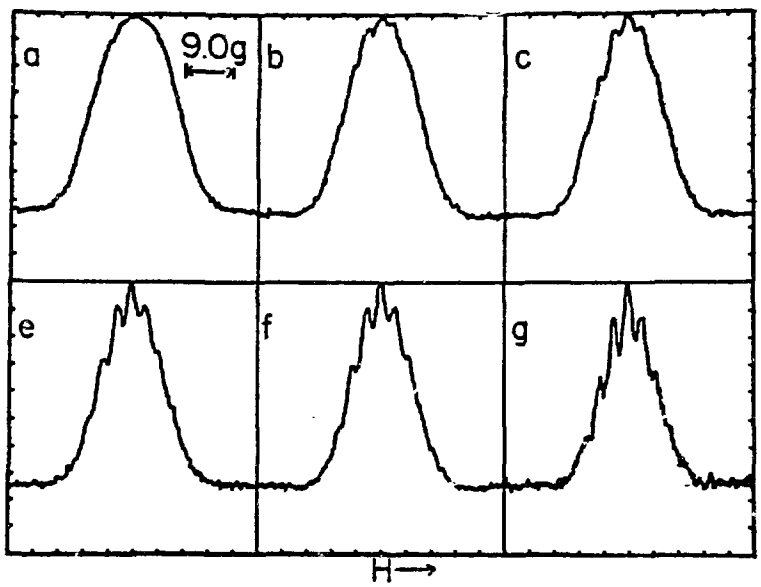

Figure 13. Microwave magnetic field (H_1) dependence of FDMR of 10^{-3} M biphenyl in cyclohexane. A microwave pulse of H_1 value 1.5 G (a), 0.74 G (b), 0.6 G (c), 0.47 G (d), 0.37 G (e) or 0.26 G (f) was applied from 0 to 500 ns after irradiation. The fluoresence was sampled from 500 to 600 ns after irradiation.

Figure 14. Comparison of fluorescence intensity (○) and FDMR intensity (●) observed in 10^{-3} M PPO-cyclohexane. A microwave pulse was applied from 0-100 ns after irradiation. The fluorescence was sampled at time Δ after the center of the microwave pulse. For comparison, the FDMR intensity has been scaled by an arbitrary multiplicative constant.

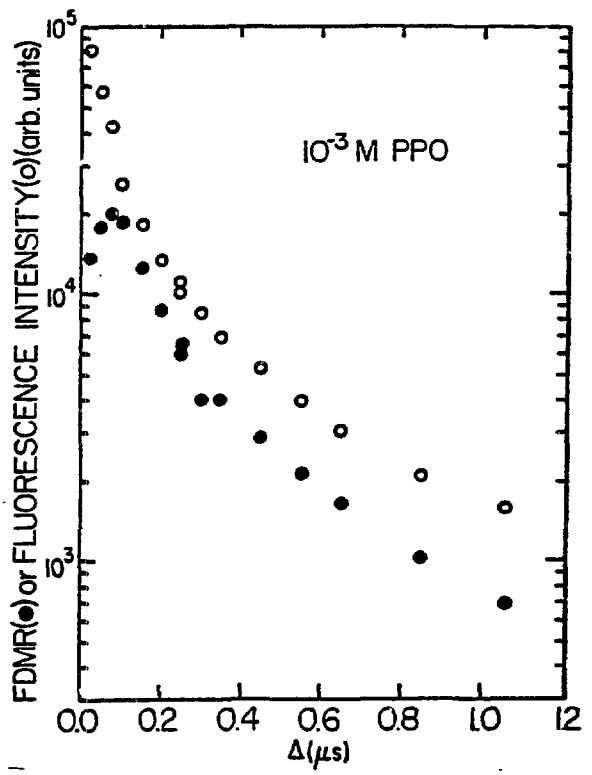

dynamics and chemical kinetics (Figure 14). The intensity of the FDMR signal increases for ~70 ns after application of the microwave pulse and then decays. The time dependence of the FDMR intensity is dominated by spin dynamics in the time domain immediately following the microwave pulse and by the recombination kinetics of the radical ion pair population at later times.

When the time dependence of the FDMR intensity is measured with higher time resolution (Figure 15), it is clear that most of the FDMR intensity develops after the microwave pulse has ended. Furthermore, compared with data for the corresponding deuterated solutes, the FDMR intensity observed in cyclohexane solutions of biphenyl-h_{10} or anthracene-h_{10} reaches a larger maximum value at an earlier time (9). This behavior can be understood in terms of the radical ion pair spin dynamics. Geminate radical ion pairs are created with purely singlet orientation of the unpaired electron spins. In a static magnetic field, the electron spin wavefunction Ψ rapidly evolves from its initial state where $|\langle\Psi|S\rangle|^2 = 1$ to a quasi steady state where $|\langle\Psi|S\rangle|^2 = |\langle\Psi|T_0\rangle|^2$ (10). Microwave radiation of the appropriate frequency connects states with T_0 character with states of T_{+1} or T_{-1} character and a decrease in $|\langle\Psi|T_0\rangle|^2$ results. After the microwave pulse, hyperfine induced S-T_0 mixing acts to re-establish the steady state at a rate determined by the magnitude of the hyperfine coupling constants. The S-T_0 mixing rate is given by:

$$\omega_{S\text{-}T_0} = (2h^{-1})[(g_1 - g_2)\beta H_0 + \sum_i a_{1i}m_{1i} + \sum_j a_{2j}m_{2j}] \qquad (12)$$

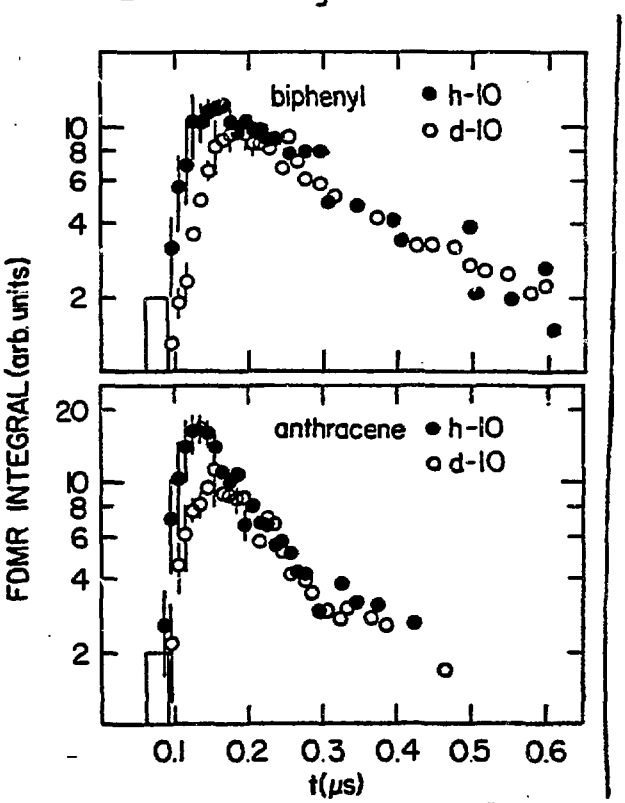

Figure 15. Time dependence of integrated FDMR intensity observed in cyclohexane solutions (0.001 M) of (a) biphenyl-h_{10} (●) and biphenyl-d_{10} (○) or (b) anthracene-h_{10} (●) and anthracene-d_{10} (○). Vertical bars represent standard deviation of the mean FDMR intensity for times where multiple spectra were measured. The rectangular box indicates the position of the 30 ns microwave pulse. The integrated area units of biphenyl and anthracene FDMR are not directly comparable.

which is the familiar expression from treatments of CIDNP, CIDEP, and the magnetic field effect (11). Since usually there is no substantial g factor difference for aromatic radical cations and anions, the hyperfine coupling constants determine the $S-T_0$ mixing rate. Consequently, in the time domain immediately following the microwave pulse, we observe the decay of $|\langle\Psi|S\rangle|^2$ as the steady state is approached. Due to the smaller hyperfine coupling constants of the deuterated radical ions, the rate of $S-T_0$ mixing, and thus the approach to the steady state is slower for deuterated solutes. After the steady state is established, the time dependence of the FDMR intensity is determined by the recombination kinetics of the radical ion pairs.

The time and radiation dose dependence of the FDMR intensity establish that the FDMR phenomenon is a resonant change in the yield of excited singlets from *geminate* ion recombination. Time resolved absorption and conductivity measurements (12,13) have shown that the yield (G_{gi}) of geminate ion pairs decays according to

$$G_{gi}(t) = G_{fi}[1 + (\gamma/t)^{\frac{1}{2}}] \qquad (13)$$

where G_{fi} is the free ion yield and γ is characteristic of the recombination reaction kinetics. If the FDMR effect is a resonant change in the yield of excited states arising from geminate recombination then the FDMR intensity should be proportional to $t^{-3/2}$ and scale linearly with the absorbed dose, since the fluorescence intensity is proportional to the number of recombination events per unit time. This behavior is observed for a broad range of radiation doses (Figure 16). At higher doses, an increased rate of decay of the FDMR intensity suggests a possible contribution by a dose dependent rate of spin lattice relaxation due to Heisenberg exchange (6).

The FDMR spectrum is sensitive to the structure of the radical ion precursors of excited states. Consequently, the FDMR technique could be used to distinguish the contributions of the various recombination pathways (9-11) to excited state production. The FDMR spectrum of the PPO-cyclohexane system at a low solute concentration shows the presence of broad "wings" in addition to a narrow central peak (Figure 17). The decay of the radical species responsible for the wings is somewhat faster than the decay of the species responsible for the central peak (6). This behavior is consistent with the idea that the wings are essentially the EPR spectrum of the cyclohexane radical cation or "hole". The kinetic properties of the species responsible for the wings are being actively investigated. If the FDMR method could be used to obtain quantitative data on the relative importance of solvent-solute or solute-solute recombination in excited state production, it could provide the first direct experimental check on theoretical calculations of the recombination kinetics (14,15).

Future applications of FDMR in radiation chemistry will explore excited state production in increasingly complex chemical systems where the sensitivity and specificity of the

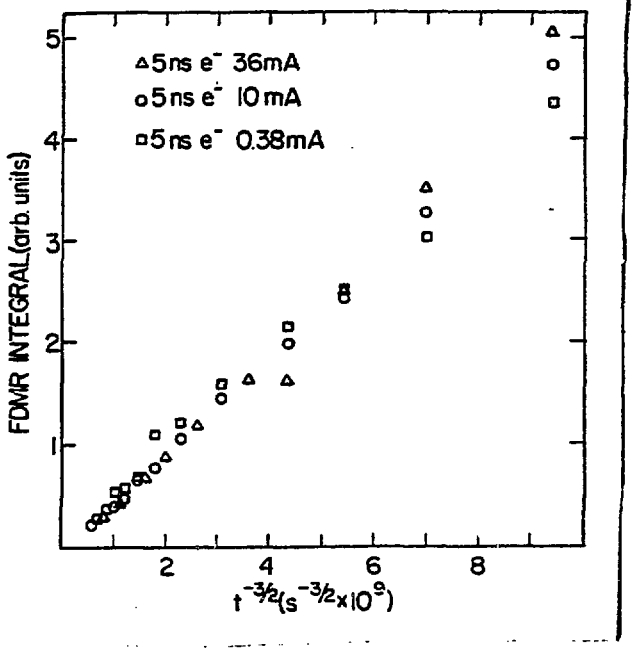

Figure 16. Radiation dose dependence of FDMR of 10^{-3} M PPO in cyclohexane plotted on a $t^{-3/2}$ scale. Samples were irradiated with 5 ns electron beam pulses with peak current values of 36 mA (△), 10 mA (○), and 0.38 m (□). The microwave pulse was applied from 0 to 100 ns after irradiation and the fluorescence was sampled at time t after irradiation. Data for different doses were scaled so that all data sets had a common value at $t^{-3/2} = 4 \times 10^9$ $s^{-3/2}$.

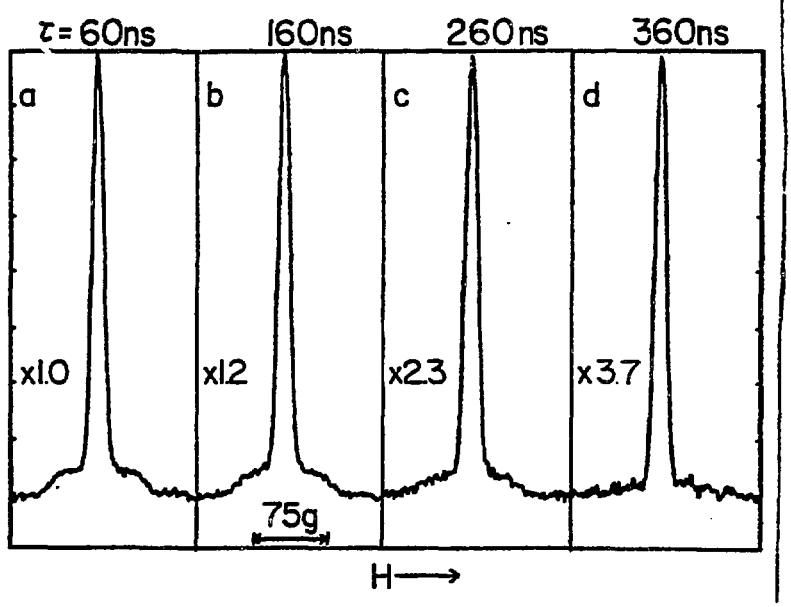

Figure 17. Dependence of the FDMR of 10^{-4} M PPO in cyclohexane wave pulse was started at 10 ns (a), 110 ns (b), 210 ns (c), and 310 ns (d) after irradiation. The fluorescence was sampled from 75 ns to 175 ns after the start of the microwave pulse. For comparison the y axis values of the spectra have been multiplied by the factors indicated.

technique can be exploited to best advantage. Another potentially fruitful area of inquiry is the recombination of photoproduced ion pairs in liquid solution. Accordingly, we have recently undertaken an FDMR investigation of photoionization induced by an excimer laser excitation source.

SUMMARY

We have illustrated time resolved pulsed EPR experiments utilizing both microwave and optical detection. We feel that, in the future, these techniques will be applied to many interesting problems in radiation and photochemistry. We have tried to illustrate, through selected examples from our recent work, how pulsed EPR methods offer significant advantages over conventional CW EPR techniques for the study of transient paramagnetic species.

ACKNOWLEDGMENT

Work supported by the Office of Basic Energy Sciences, Division of Chemical Sciences, U. S. Department of Energy, under Contract W-31-109-Eng-38.

REFERENCES

(1) A. D. Trifunac and M. C. Thurnauer, *Time Domain Electron Spin Resonance*, Ch. 4, ed. L. Kevan and R. N. Schwartz, John Wiley & Sons, Inc., New York, 1979.
(2) A. D. Trifunac and J. R. Norris, Chem. Phys. Lett. 59, 140 (1978).
(3) A. D. Trifunac, J. R. Norris, and R. G. Lawler, J. Chem. Phys. 71, 1380 (1979).
(4) N. C. Verma and R. W. Fessenden, J. Chem. Phys. 65, 2139 (1976).
(5) A. D. Trifunac and J. P. Smith, Chem. Phys. Lett. 73, 94 (1980).
(6) J. P. Smith and A. D. Trifunac, J. Phys. Chem. 85, 1645 (1981).
(7) C. D. Jonah, M. C. Sauer, Jr., R. Cooper, and A. D. Trifunac, Chem. Phys. Lett. 63, 535 (1979).
(8) Y. Katsumara, S. Tagawa, Y. Tabata, J. Phys. Chem. 84, 833 (1980).
(9) J. P. Smith and A. D. Trifunac, Chem. Phys. Lett., in press (1981).
(10) B. Brocklehurst, J. Chem. Soc. Faraday Trans. II, 72, 1869 (1976).
(11) For a general reference see *Chemically Induced Magnetic Polarization*, L. T. Muus *et al.*, eds., D. Reidel Publishing Co., Holland and USA, 1977.
(12) J. M. Warman, P. P. Infelta, M. P. DeHaas, A. Hummel, Can. J. Chem. 55, 2249 (1977).
(13) C. A. M. Van Den Ende, L. Nyikos, J. M. Warman, and A. Hummel, Radiat. Phys. Chem. 15, 273 (1980).
(14) S. J. Rzad, J. Phys. Chem. 76, 3722 (1972).
(15) M. C. Sauer, Jr. and C. D. Jonah, J. Phys. Chem. 84, 2539 (1980).